Magnetic properties of In_2O_3 containing Fe_3O_4 nanoparticles

Marzook S. Alshammari,[1,2,*] Mohammed S. Alqahtani,[1,3] Hasan B. Albargi,[1] Salman A. Alfihed,[2] Yaser A. Alshetwi,[2] Abdulrahman A. Alghihab,[2] Abdullah M. Alsamrah,[2] Nawaf M. Alshammari,[2] Mohammed A. Aldosari,[2] Ahmed Alyamani,[2] Ali M. H. R. Hakimi,[4] Steve M. Heald,[5] Harry J. Blythe,[1] Mark G. Blamire,[4] A. Mark Fox,[1] and Gillian A. Gehring[1,*]

[1]*Department of Physics and Astronomy, University of Sheffield, Sheffield S3 7RH, United Kingdom*

[2]*The National Center of Nanotechnology, King Abdulaziz City for Science and Technology, Riyadh 11442, Saudi Arabia*

[3]*Department of Physics and Astronomy, King Saud University, Riyadh 11451, Saudi Arabia*

[4]*Department of Materials Science and Metallurgy, University of Cambridge, 27, Charles Babbage Road, Cambridge, CB3 0FS*

[5]*Advanced Photon Source, Argonne National Laboratory, Argonne, Illinois 60439, USA*

(Received 6 February 2014; revised manuscript received 28 July 2014; published 28 October 2014)

Films of Fe-doped In_2O_3 that were deliberately fabricated so they contained Fe_3O_4 nanoparticles were deposited on sapphire substrates by pulsed laser deposition at low oxygen pressure. The concentration of Fe was varied between 1% and 5%, and the effect of including 5% of Sn and vacuum annealing were also investigated. Structural analysis indicated a high concentration of Fe_3O_4 nanoparticles that caused substantial values of the coercive field at room temperature. Transport measurements indicated that the films were metallic, and an anomalous Hall effect was observed for the sample with 5% of Fe. The concentration of nanoparticles was reduced dramatically by the inclusion of 5% of Sn. Magnetic circular dichroism spectra taken in field and at remanence were analyzed to show that the samples had a magnetically polarized defect band located below the conduction band as well as magnetic Fe_3O_4 nanoparticles. The signal from the defect states near the band edge was enhanced by increasing the number of carriers by either including Sn or by annealing in vacuum.

DOI: 10.1103/PhysRevB.90.144433 PACS number(s): 75.50.Pp, 78.20.Ls, 81.07.−b, 75.47.Lx

I. INTRODUCTION

The study of doped magnetic oxides that have robust magnetism at room temperature (RT) has been pursued energetically in recent years because of the possibility of their use in spintronic devices [1,2]. The semiconductor In_2O_3 has a cubic bixbyite structure and is transparent in the visible region; it is widely used in semiconductor devices particularly when it is doped with Sn (ITO) to make it more conductive [3–6]. If grown stoichiometrically, it appears to be *n*-type because of a surface charge density; however, if the carrier concentration is enhanced by the addition of Sn or if it was grown oxygen deficient, then the carriers reside in the bulk [7,8].

Recently there have been a number of papers reporting ferromagnetism in In_2O_3 films [9–16] doped with transition metal ions. In many oxides there has been a debate over the question of whether the magnetism is due to intrinsic properties of the host matrix containing transition metal ions on the cation sites or whether the magnetism is due to impurity phases. This controversy has also existed for Fe-doped In_2O_3 where the expected impurity phase is Fe_3O_4. Some authors have reported that the Fe enters the lattice substitutionally for concentrations as high as 20% [14,15] so that the magnetism is intrinsic; however, there are also reports that the magnetism is due to ferromagnetic inclusions of Fe_2O_3 [17]. Some films have also been made to contain nanophases of Fe_3O_4 by including nanoparticles in the target for pulsed laser deposition (PLD) [18] or by using a special substrate [19]. A number of studies have used assembled nanoparticles of Fe_3O_4 that were sufficiently small that they would be in the superparamagnetic regime at RT in order to study the magnetoresistance [20–23].

In this paper we investigate the relative importance to the magnetic properties of Fe_3O_4 nanoparticles and magnetically polarized bands of In_2O_3 [24–27]. We used a fabrication method that would produce films containing nanoparticles and controlled them by adding Sn. Optical studies are a very powerful tool to investigate the polarization of defect bands associated with donor levels [27] and also to determine the contribution from defect phases [28] and have been used extensively here to characterize our films. In this paper we report on the growth and structural characterization of films of Fe-doped In_2O_3 and ITO in Secs. II and III. The electronic transport properties, magnetization, optical absorption, and magneto-optical spectra are reported in Secs. IV, V, VI, and VII. The results of these investigations are discussed in Secs. VIII and IX and show that the magnetization originates in both the Fe-doped In_2O_3 lattice and also in the nanoparticles of Fe_3O_4.

II. SAMPLE PREPARATION

In this work the films were deliberately made to include nanoparticles of Fe_3O_4 to contrast with earlier studies for which the material for the targets was ground by hand so that Fe_3O_4 inclusions would be absent [10]. The targets for PLD were made by a solid-state reaction method from In_2O_3 (99.99%), Fe_2O_3 (99%), and, when appropriate, SnO_2 (99.99%) powders using a sequence of milling and annealing. The powders were mixed to the required ratios, milled, and then annealed at 400 °C; the mixture was milled again and annealed at 600 °C; and then milled again for a third time

*Corresponding authors: alshammari@kacst.edu.sa, g.gehring@shef.ac.uk

TABLE I. The actual concentration of Fe in In_2O_3 thin films measured by EDAX.

% of Fe in the target	EDAX measurement of % Fe in the film
1	0.89%
2	1.72%
3	2.99%
4	4.07%
5	5.03%

and annealed at 800 °C and milled again. All the milling was performed using SiN vial and balls for 30 minutes at a speed of 300 rpm using 1:20 mass ratio for the powder to the balls, and the annealing was done for 8 hours with a ramp rate of 5 °C/min. Finally, 8.5 g of the mixture was compressed at 40 000 kPa using 3 drops of Gelisrin to make targets of 25 mm diameter and 5 mm thickness. The resultant targets were sintered at 900 °C for 8 hours with a ramp rate of 5 °C/min.

The thin films were deposited by PLD on sapphire substrates (0001) at a growth temperature of 600 °C using a KrF (248 nm) excimer laser with pulse duration of 20 ns, a repetition rate of 10 Hz, and an energy of 250 mJ. The oxygen partial pressure was sustained at 2×10^{-3} mTorr during the growth process. The thicknesses of the films varied between 160 nm and 330 nm.

In the first series of films, the concentration of Fe varied from 1% to 5%; the concentrations were measured by energy dispersive x-ray analysis (EDAX) and the results are given in Table I. As they were equal to those of the target within the errors, the films are referred to by their nominal composition; however, the measured values have been used in the plots of measured quantities against composition.

It was found that the films made with 5% Fe had the largest magnetization (see Sec. V), and so two other series of films were made with 5% Fe. One set of films was annealed in vacuum to increase the density of oxygen vacancies. The vacuum annealing was done at temperatures of 300 °C, 400 °C, and 500 °C for 30 minutes. Another set of films was grown with 5% Fe and with 5% of Sn.

III. STRUCTURAL ANALYSIS

Figure 1 presents the results of an x-ray diffraction (XRD) analysis of the films using an x-ray source of CuK_α (λ = 0.15406 nm). The results showed that the films were highly crystalline and well oriented along (222) in agreement with an earlier paper [10].

The lattice parameter varied nonsystematically between 1.0116 nm and 1.0126 nm rather than monotonically with Fe concentration, as reported when all the Fe was substituted on the In sites [10]. Weak reflections were observed from Fe_3O_4, as shown in Fig. 1(a), indicating the presence of the nanoparticles: the other weak lines in the spectrum are due to higher order reflections from In_2O_3 and the substrate, Al_2O_3. Scanning electron microscopy (SEM) scans were made of the samples to investigate the size of the nanoparticles. The sizes of the nanoparticles were found to be 30 ± 5 nm as shown in Fig. 1(b) for the film with 5%.

The existence of the Fe_3O_4 inclusions was also measured quantitatively by extended x-ray absorption fine structure (EXAFS) measurements made at beamline 20-ID at the Advanced Photon Source at the Argonne National Laboratory on the film containing 5% Fe. The measurements were made using fluorescence detection at a glancing angle of about 5° using a Si (111) monochromator with an energy resolution of 0.9 eV at the Fe *K* edge. Both the near edge and EXAFS spectra are very similar to those from pure Fe_3O_4, as shown in Fig. 2, indicating that approximately 85% of the Fe had the coordination characteristic of Fe_3O_4. An earlier paper had suggested that nanoclusters seen in PLD grown films of $(In_{1-x}Fe_x)_2O_3$ were Fe_2O_3 [15], but this was not seen here. The near edge shows a slight shift to lower energy, indicating the possibility of a small amount of additional Fe(2+) or Fe(0). Linear combination fitting indicated that this was most likely Fe(2+) rather than metallic Fe. The small amount (~10%)

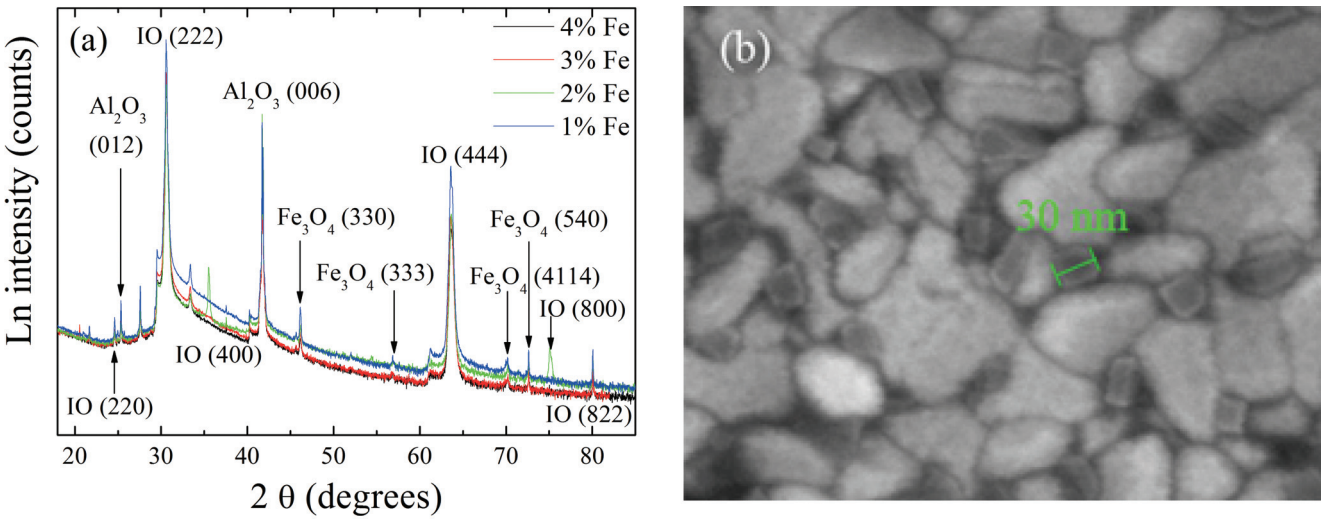

FIG. 1. (Color online) (a) XRD intensities for films with varying percentages of Fe done with a long scan time and plotted logarithmically. (b) SEM scan done at 5 kV of the 5% sample. The dark areas indicate the Fe_3O_4.

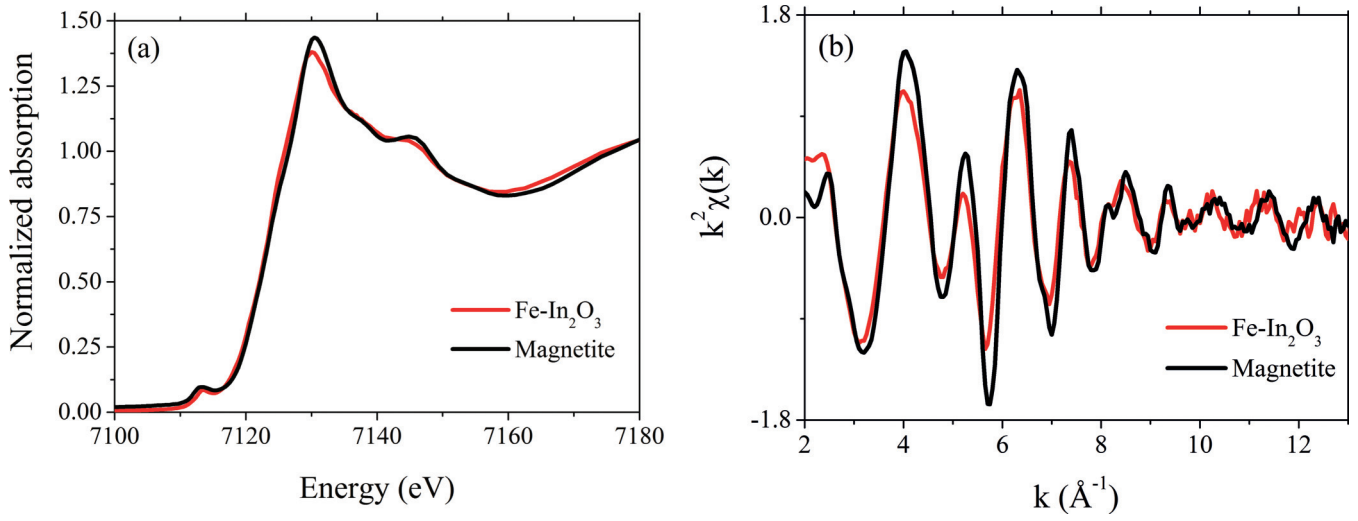

FIG. 2. (Color online) Fe K edge data for the 5% Fe In_2O_3 sample compared to Fe_3O_4 magnetite; (a) normalized near edge and (b) k^2 weighted EXAFS.

of this second phase precluded a definitive identification from this measurement; however, the magnetic circular dichroism (MCD) data, presented in Sec. VII demonstrates that any concentration of metallic Fe must be very small.

IV. TRANSPORT PROPERTIES

Measurements were made of the temperature dependence of the resistivity and the Hall effect at RT and low temperatures. All the films showed metallic behavior above ~100 K and a small rise in resistance at low temperatures that may be due to the electrical properties of the Fe_3O_4 nanoparticles below the Verwey transition at T_v = 110–125 K [29]. The resistance of the film with the lowest carrier concentration is shown in Fig. 3(a) as a function of temperature. The films with higher Fe content ($x > 0.03$) have higher carrier densities, as shown in Fig. 3(b), which suggest that the number of oxygen vacancies increases as Fe is added. Some direct evidence for this will be given from the analysis of the optical spectra. The mobility, shown in Fig. 3(c), is higher than is usually seen in Fe substitutionally doped In_2O_3 films [10] (see Secs. VI and VII). It is higher at low temperature, which is again consistent with metallic behavior and falls with increasing concentration of Fe.

V. MAGNETIC PROPERTIES

Measurements of the magnetic hysteresis loops were made with a superconducting quantum interference device (SQUID) magnetometer. Figures 4(a)–4(c) show, respectively, the hysteresis loops with the contribution from the substrate subtracted, the variation of the saturation magnetization, and the variation of the coercive field all measured with the magnetic field in the sample plane. Field-cooled (FC) and zero-field-cooled (ZFC) magnetization and the comparison of in-plane and out-of-plane data are shown in Figs. 4(d) and (e), respectively.

The saturation magnetization, shown in Fig. 4(b), is proportional to the concentration, which is unlike what is generally seen for substitutional Fe [9,10] but is consistent with most of the magnetization coming from the nanoinclusions of Fe_3O_4. The values of H_c are all considerably higher than those found for samples without Fe_3O_4 [10] but are only slightly enhanced for those measured in the perpendicular geometry. This indicates that the average over the nanoparticles is approximately isotropic [30].

The most dramatic difference between the magnetic properties when measured with the field in and out of the film plane is in the value of the saturation magnetization, which is considerably enhanced when the field is applied perpendicular to the plane. Such behavior has been seen before in doped ZnO [31]. This behavior cannot be attributed to the nanoparticles but rather to the magnetic behavior of the In_2O_3 with some Fe on In sites.

The magnetization measured in the FC/ZFC configuration indicated the presence of Fe_3O_4 with a Verwey transition occurring at $T_v \sim 115$ K [20] in the $x = 5\%$ film. Above this temperature the film behaves like a ferromagnet. (The observations that H_c at 300 K was still substantial, 400 Oe, and the fact that above 115 K the magnetization was not falling like 1/T in the ZFC plot indicated that we do not have superparamagnetic nanoparticles above 115 K; indeed, this would not be expected for nanoparticles with sizes of several tens of nanometers.) It is clear that the presence of Fe_3O_4 is having a strong effect on the magnetization and coercive field, which has resulted in a conducting sample with a high coercive field at RT.

The film with 5% Fe, which had the largest magnetization and coercive field, also showed an anomalous Hall effect (AHE) at $T = 10$ K as shown in Fig. 5. An AHE had been seen previously in films of In_2O_3 and ITO [16,32] that contained only substitutional Fe. This may indicate that although most of the magnetization originated from the Fe_3O_4 nanoparticles, the conduction electrons were also spin polarized as was observed in ITO [14], and although the strict criteria that should be satisfied for a homogenous ferromagnet (i.e., that the loops from AHE and bulk magnetization agreed and that the AHE scaled with the conductivity [33]) were not satisfied, a

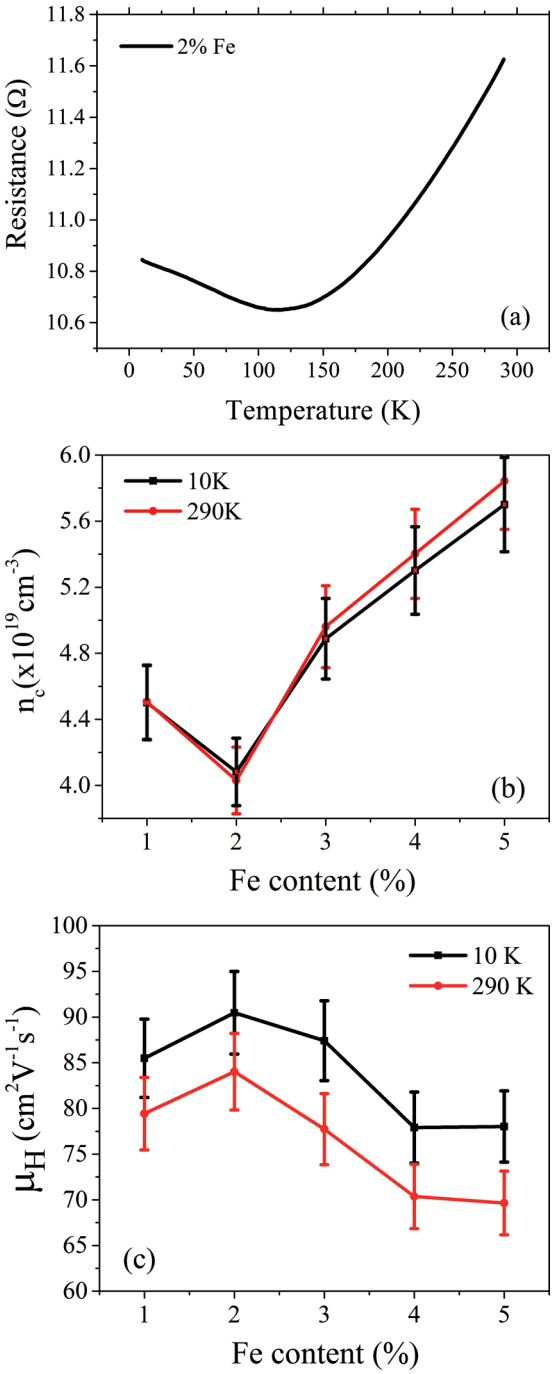

FIG. 3. (Color online) (a) The resistivity plotted as a function of temperature for a 2% Fe film, (b) carrier concentration, and (c) the Hall mobility of the films as a function of Fe concentration.

strong contribution from the nanoparticles is implied here. The coercive field of 1200 ± 200 Oe observed in the AHE was considerably higher than that observed from direct measurements, as shown in Fig. 4(c), and will be discussed in Sec. VIII. The films discussed here did not show any substantial magnetoresistance, unlike those where large effects had been seen with small implanted nanoparticles of Fe_3O_4 in ITO [18].

The carrier concentration is increased by including Sn and also by vacuum annealing; however, the effects on the magnetizations of these films are very different for these two modifications. Films grown using 5% Sn and 5% Fe had substantially lower magnetization and lower coercive field than the 5% Fe films without Sn. The saturation magnetizations with and without Sn were 8 emu/cm^3 and 22.6 emu/cm^3, respectively, and the coercive fields changed from 632 Oe to 205 Oe at 5 K and 433 Oe to 120 Oe at 300 K. However, the RT magnetization was enhanced by ∼40% for all the films that had been annealed in vacuum independent of the temperature of the annealing (300 °C, 400 °C, 500 °C), and at low temperature the coercive field increased substantially for the films annealed at 400 °C and 500 °C.

VI. REFLECTIVITY AND ABSORPTION MEASUREMENTS

Optical studies are a powerful technique to determine the energy structure of these doped films. Measurements were made to complement those of the magnetization at RT using a xenon lamp and monochromator with a photomultiplier tube detector in the range of energies of spectra between 1.7 and 4.5 eV. Optical absorption measurements were made to ascertain how the band gap varied with Fe concentration and also to detect the contribution from the absorption of the Fe_3O_4 nanoparticles and the unoccupied donor levels below the conduction band. Reflection and absorption data are shown in Fig. 6. The reflection data in Fig. 6(a) shows oscillations from standing waves in the thin films, which are a characteristic of good quality films with low absorption; however, the minimum value of the reflectivity is higher than 0.11, which corresponds to the reflection from the substrate [34], which indicates that there is some scattering consistent with the observed surface roughness. The scattering from the film surface is contributing to the apparent absorption below 3 eV.

Fe-doped In_2O_3 thin films show absorption below the optical absorption edge around 3.3 eV where the formation of oxygen vacancy bands is expected. There is also some absorption at lower energy, which is expected from the Fe_3O_4 nanoparticles. The optical absorption edge, determined from a plot of α^2, is shown in the inset of Fig. 6(b). Annealing the films and also adding Sn causes more absorption below the band gap. The energy gap increases with the addition of Sn as expected [35].

VII. MAGNETO-OPTICAL PROPERTIES

The magnetic circular dichroism (MCD), which is the difference in absorption between left and right circularly polarized light, measured in Faraday geometry, complements the absorption measurements presented in Sec. VI. The spectra were taken at energies between 1.5 and 4.2 eV using a xenon lamp and monochromator with a photoelastic modulator. The measurements were taken at RT in an applied magnetic field of 1.8 T and at remanence (after reducing the field to zero from ±1.8 T). The MCD of a sapphire substrate was measured in field, and the result subtracted from the film spectra that were taken in field. The remanence spectrum does not require this correction.

The MCD spectra are shown in Fig. 7 as a function of Fe concentration with characteristic features near 2.0 eV and

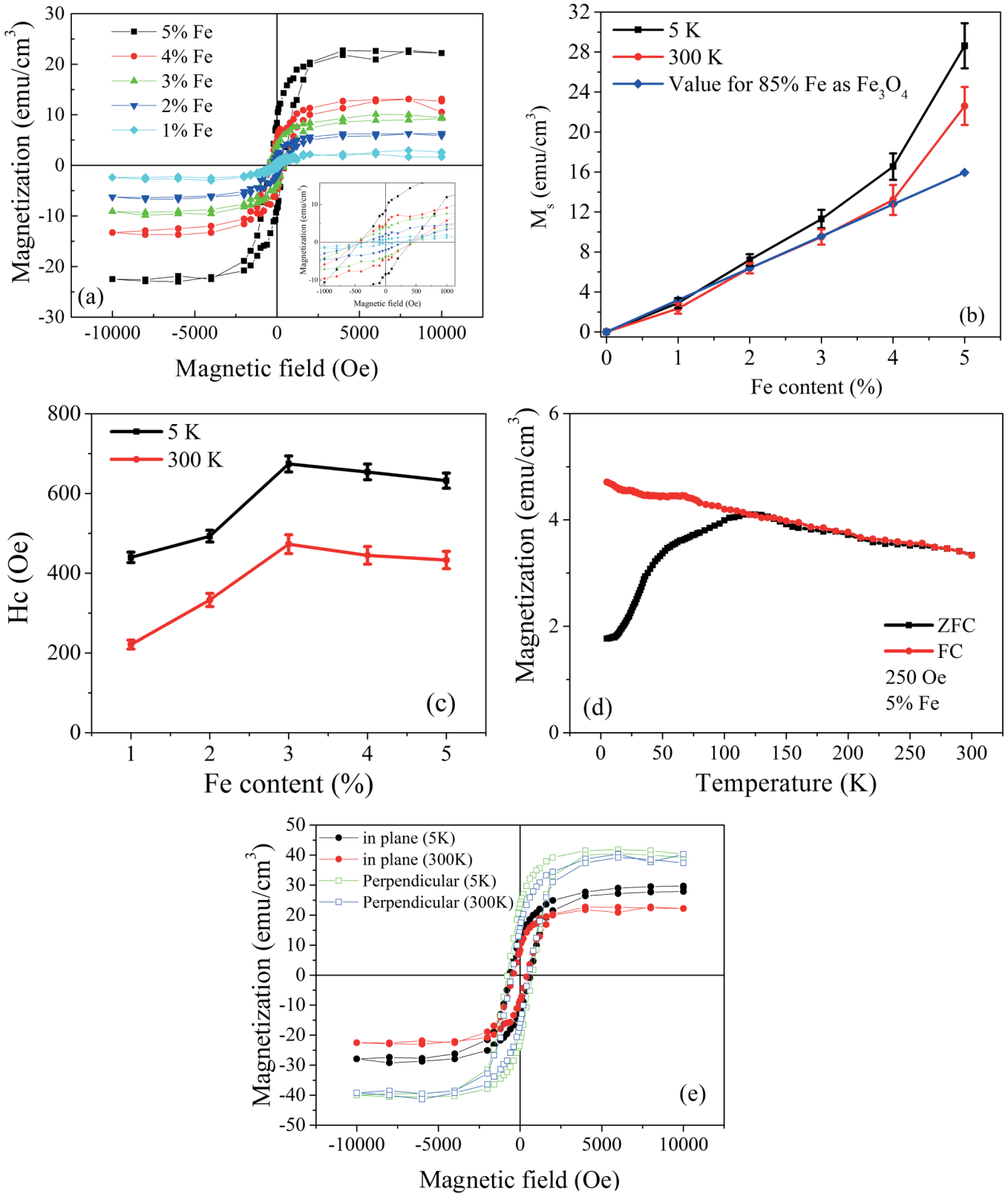

FIG. 4. (Color online) (a) Hysteresis loops measured at 300 K of $(In_{1-x}Fe_x)_2O_3$ with the field in plane (the diamagnetic contribution from the substrate has been subtracted).The inset shows an expanded view of the region around the origin. (b) The saturation magnetization at 5 K and 300 K as a function of the Fe doping level compared with expected magnetization from 85% of Fe in the films in the form of Fe_3O_4. (c) The coercive field, H_c, at 5 K and 300 K as a function of the measured Fe doping level. (d) ZFC and FC magnetization of $(In_{0.95}Fe_{0.05})_2O_3$ film, taken at 250 Oe, as a function of temperature. (e) Comparison of the hysteresis loops taken for the 5% sample with the field in plane and perpendicular to the plane.

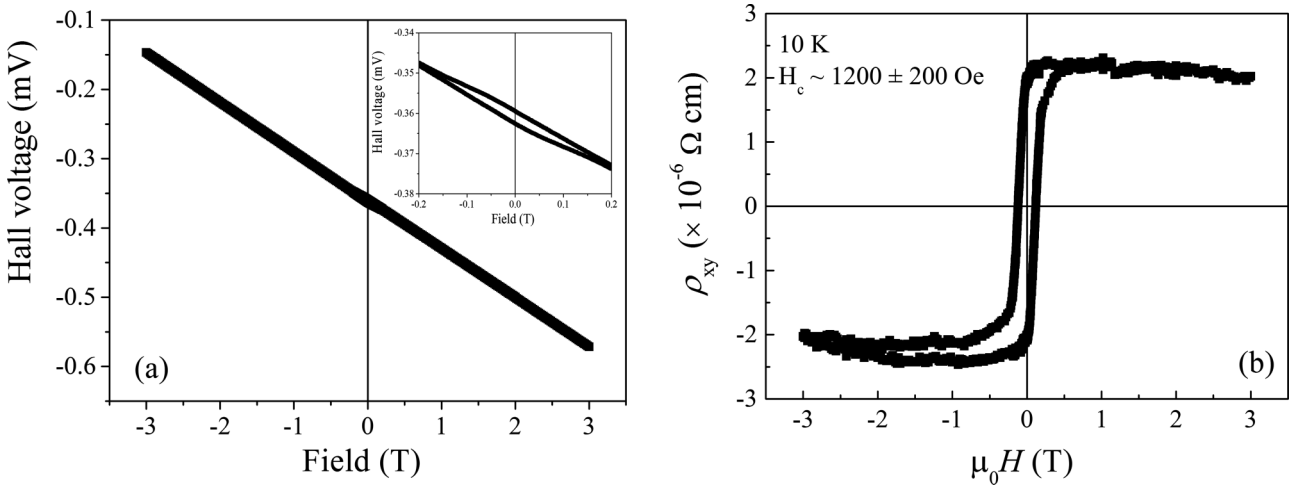

FIG. 5. Hall effect measurements of the 5% film measured at 10 K. Raw data are shown in (a), and the result when the linear term is subtracted in (b).

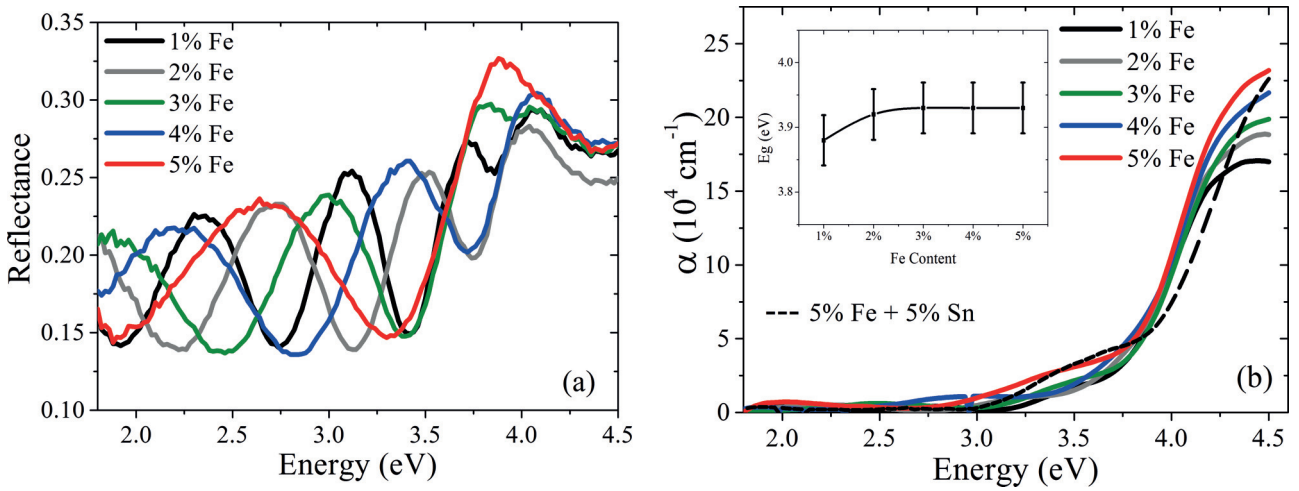

FIG. 6. (Color online) (a) Optical reflection spectra and (b) absorption spectra for $(In_{1-x}Fe_x)_2O_3$ thin films with varying Fe content; the band gaps are shown in the inset.

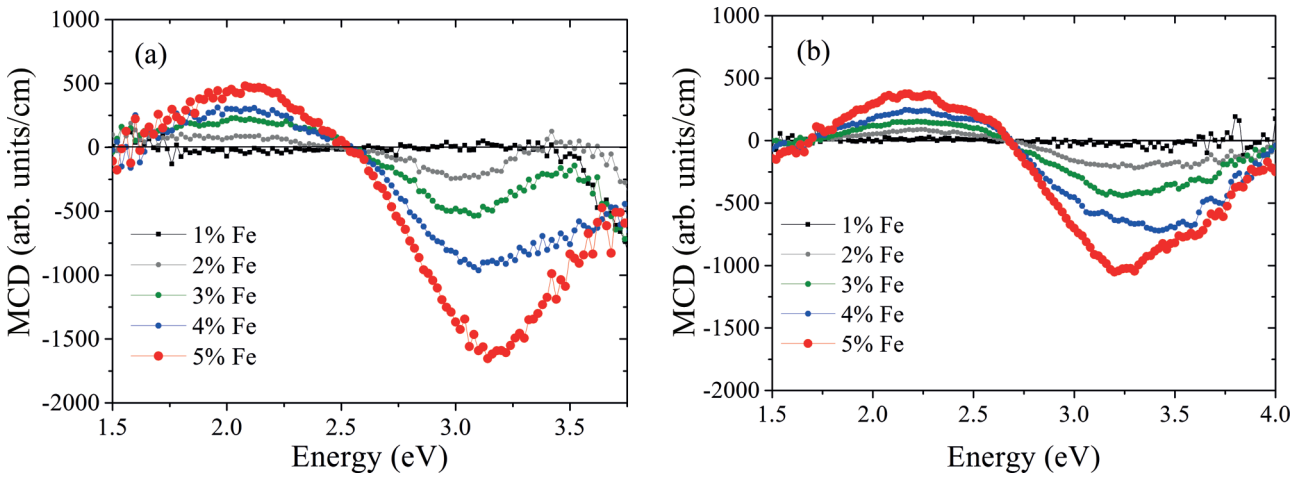

FIG. 7. (Color online) MCD spectra of $(In_{1-x}Fe_x)_2O_3$ thin films (a) in an external applied field of 1.8 Tesla, (b) at remanence (in magnetic field of 0 T) measured at RT. The contribution from the substrate was subtracted from the data.

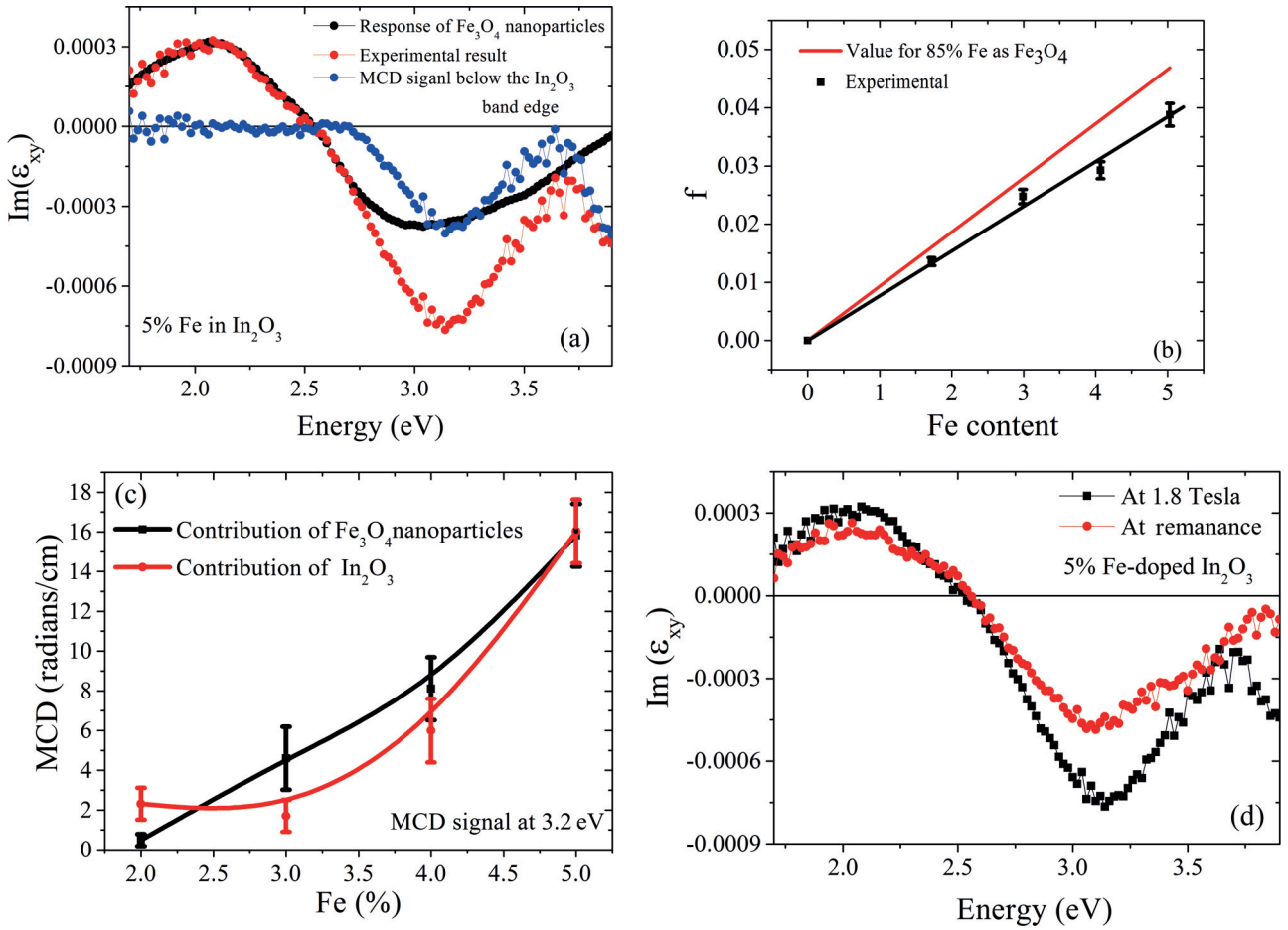

FIG. 8. (Color online) (a) MCD data for a $(In_{0.95}Fe_{0.05})_2O_3$ thin film measured at RT and magnetic field of 1.8 T. The red line represents the experimental value of the imaginary part of the off-diagonal dielectric tensor. The black line is a fit to the contribution from the Fe_3O_4 nanoparticles using Maxwell-Garnett theory, while the difference (blue line) is the contribution from the In_2O_3 matrix. (b) The values of the volume fraction f corresponding to nanoparticles as computed from the MCD (black line) and the value obtained from EXAFS measurements on the 5% film (red line) plotted against the measured percentage of Fe. (c) Variation in the MCD amplitude at 3.2 eV with Fe content for Fe_3O_4 nanoparticles and the oxide component. The lines in (b) and (c) are to guide the eye. (d) The MCD data for 5% Fe sample at 1.8 T and at remanence.

3.2 eV. The feature above ∼3 eV is characteristic of oxide magnetism occurring under the band gap [10,27,36] and arises from transitions to gap states localized either on oxygen vacancies or on grain boundaries.

We expect a signal from the Fe_3O_4 nanoparticles. The Maxwell-Garnett theory [37,38] is used to evaluate the effective dielectric constant for Fe_3O_4 nanoparticles embedded in an In_2O_3 matrix. The result is given in terms of the dielectric tensor for Fe_3O_4 and In_2O_3, which is taken as the refractive index n squared, the shape factor of the nanoparticles, L_{xx}, and the fraction of the volume, f, that is occupied by nanoparticles,

$$\tilde{\varepsilon}_{xy}^{\text{eff}} = \frac{f\left(\tilde{\varepsilon}_{xy}^{Fe_3O_4}\right)}{\left[1 + \frac{L_{xx}}{n^2}\left(\tilde{\varepsilon}_{xx}^{Fe_3O_4} - n^2\right)\right]^2}. \quad (1)$$

The MCD is used to obtain an experimental expression for $\text{Im}\tilde{\varepsilon}_{xy}^{\text{expt}}$ $\text{MCD} = \frac{\pi l}{\lambda n}\text{Im}\tilde{\varepsilon}_{xy}^{\text{expt}}$ used where l is the film thickness, λ is the light wavelength, and n the refractive index of In_2O_3. The experimental spectrum of $\text{Im}\tilde{\varepsilon}_{xy}^{\text{expt}}$ is compared with that expected from the nanoparticles in Fig. 8(a) using published results [39] for the refractive index, n, $\tilde{\varepsilon}_{xx}^{Fe_3O_4}$, and $\tilde{\varepsilon}_{xy}^{Fe_3O_4}$. The parameters f and L_{xx} were fitted in the energy range $1.5 < E < 2.7$eV. There is an additional signal near the band edge that is attributed to the doped In_2O_3, $\tilde{\varepsilon}_{xy}^{In_2O_3}$. Hence the expression for the total $\text{Im}\tilde{\varepsilon}_{xy}^{\text{expt}}$ is given by

$$\text{Im}\tilde{\varepsilon}_{xy}^{\text{expt}} = \text{Im}\tilde{\varepsilon}_{xy}^{In_2O_3} + \text{Im}\tilde{\varepsilon}_{xy}^{\text{eff}}. \quad (2)$$

The fit is good using bulk values for $\tilde{\varepsilon}_{xy}^{\text{eff}}$, which means that any modification to $\tilde{\varepsilon}_{xy}$ due to the finite size of the nanoparticles has been neglected. The value of L_{xx}, which is found from the fit, was 0.33 (corresponding to an isotropic array of nanoparticles) for all values of $x > 1\%$; this is in agreement with the isotropy of the coercive field shown in Fig. 4(e). The values of f found from the fitting of the MCD is compared with the value found from the EXAFS measurement of the 5% sample in Fig. 8(b). We use this to estimate that the fraction of the Fe ions that are in ferromagnetic nanoparticles is ∼67% for all concentrations of Fe. This is smaller than ∼85% of Fe ions that were observed to have coordination of Fe_3O_4 using EXAFS because MCD measures only the parts of the clusters of Fe_3O_4 that have the magneto-optic response of the bulk whereas the EXAFS is a structural study.

TABLE II. Summary of the magnetization, MCD for Fe-doped In_2O_3 thin films at 300 K. M_s denotes the saturation magnetization, M_r the remanent magnetization, MCD_s and MCD_r the magnetic circular dichroism in field ($H > 0$) and at remanence ($H = 0$), respectively.

Fe (%)	M_s (300 K) (emu cm^{-3})	M_r (300 K) (emu cm^{-3})	M_r/M_s (300K)	MCD_r/MCD_s (2 eV, 300 K)	MCD_r/MCD_s (3.2 eV, 300 K)
1	2.34 ± 0.25	0.68 ± 0.07	0.29 ± 0.05	0.91 ± 0.03	0.91 ± 0.03
2	6.37 ± 0.64	2.12 ± 0.15	0.33 ± 0.04	0.98 ± 0.02	0.90 ± 0.02
3	9.5 ± 0.71	3.95 ± 0.28	0.42 ± 0.04	0.78 ± 0.05	0.84 ± 0.03
4	13.21 ± 0.92	4.26 ± 0.20	0.32 ± 0.03	0.85 ± 0.03	0.72 ± 0.05
5	22.6 ± 0.1.13	8.44 ± 0.60	0.37 ± 0.03	0.81 ± 0.04	0.63 ± 0.04

These data could also be used to eliminate the possibility that the films contained a significant fraction of metallic Fe because the MCD of Fe inclusions in In_2O_3 gives a negative contribution to the MCD between 2 eV and 3 eV, which is incompatible with the observed zero of the MCD at 2.5 eV [40].

We characterized the relative magnitude of the MCD signal from the polarized In_2O_3 matrix by its value at 3.2 eV; it is seen in Fig. 8(c) that both components increase with increasing x (these have been scaled so that they agree at 5%). This agrees with the increase in the observed magnetization and also in the number of carriers with x. The bulk magnetization for the 5% film changes rather little with temperature; the MCD was also found to be similarly constant as the temperature was lowered (not shown).

The MCD can be used to separate the behavior of the magnetization from the Fe_3O_4 nanoparticles from that of the polarized matrix. The MCD taken at remanence is compared to that taken at saturation in Fig. 8(d). It is seen that the band edge signal is reducing significantly more than that due to the Fe_3O_4. This is a different scenario from that observed in Co-doped In_2O_3 where there was no signal indicating any nanoparticles and the MCD follows the bulk hysteresis curve [41].

We compare the MCD signals at 2 eV where the oxide signal from the band edge signal is negligible. In Table II, we compare the ratio of these MCD signals with the ratio of the remanent to saturation magnetization. We see that MCD at 2 eV is far more robust than that of the saturation magnetization. This implies that there is another contribution to the saturated magnetization that does not contribute so much at remanence. We note that in the remanent spectrum the energy where $\mathrm{Im}\tilde{\varepsilon}_{xy}^{\mathrm{eff}} = 0$ has increased corresponds to an increase in L_{xx}, which means that at remanence more of the magnetization resides in nanoparticles that are elongated along the normal to the film, as might be expected from magnetostatic considerations.

The effect of doping the films with 5% Sn, gives a dramatic change in the MCD as shown in Fig. 9(a). The signal from the Fe_3O_4 nanoparticles has essentially vanished and the band edge signal is enhanced strongly. This is significant because the coercive field drops to values typical of Fe-doped In_2O_3 without nanoparticles (205 Oe at 5 K and 120 Oe at 300 K), but the magnetization dropped from 22 emu/cm^3 without Sn to 8 emu/cm^3 with Sn and without nanoparticles.

Annealing the films in vacuum had a different effect. It is seen in Fig. 9(b) that the contribution from the polarized carriers is increased substantially; however, there is only a small increase in the contribution from the Fe_3O_4 nanoparticles. Thus in both cases, vacuum annealing and doping with Sn, the band edge signal is enhanced commensurate with the increase in the number of donor states and carrier density. However, the presence of Sn also had the interesting effect of reducing the density of nanoparticles strongly, and this had a dramatic effect on the coercive field as noted above.

Hysteresis loops are obtained using the MCD, which is done with the magnetic field perpendicular to the plane, as is the AHE. A particular interest is a comparison of the

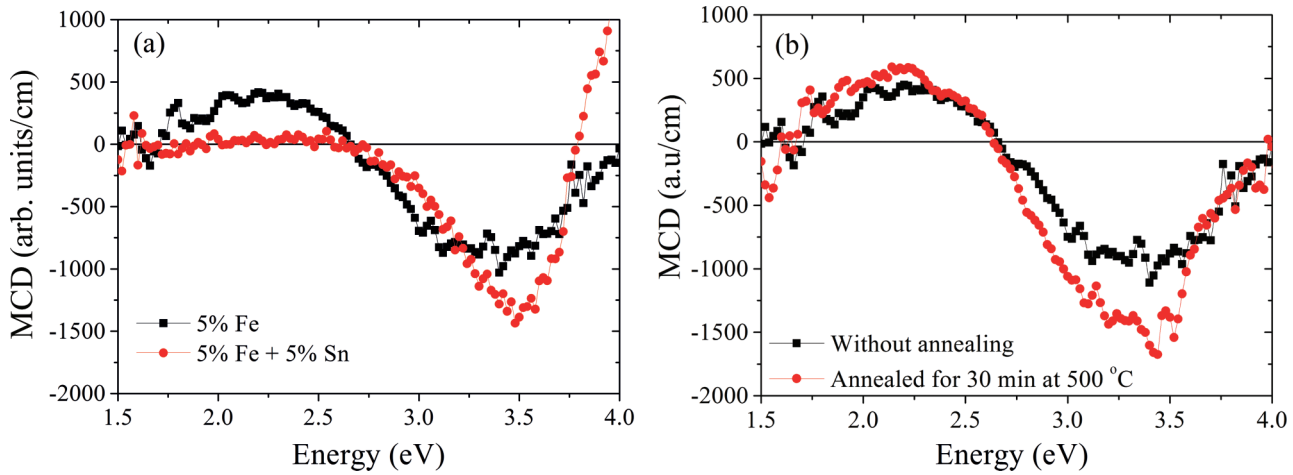

FIG. 9. (Color online) (a) Variation in the MCD spectrum of $(In_{0.95}Fe_{0.05})_2O_3$ thin films with varying tin content. (b) Variation in the MCD spectra of $(In_{0.95}Fe_{0.05})_2O_3$ thin films with annealing temperature

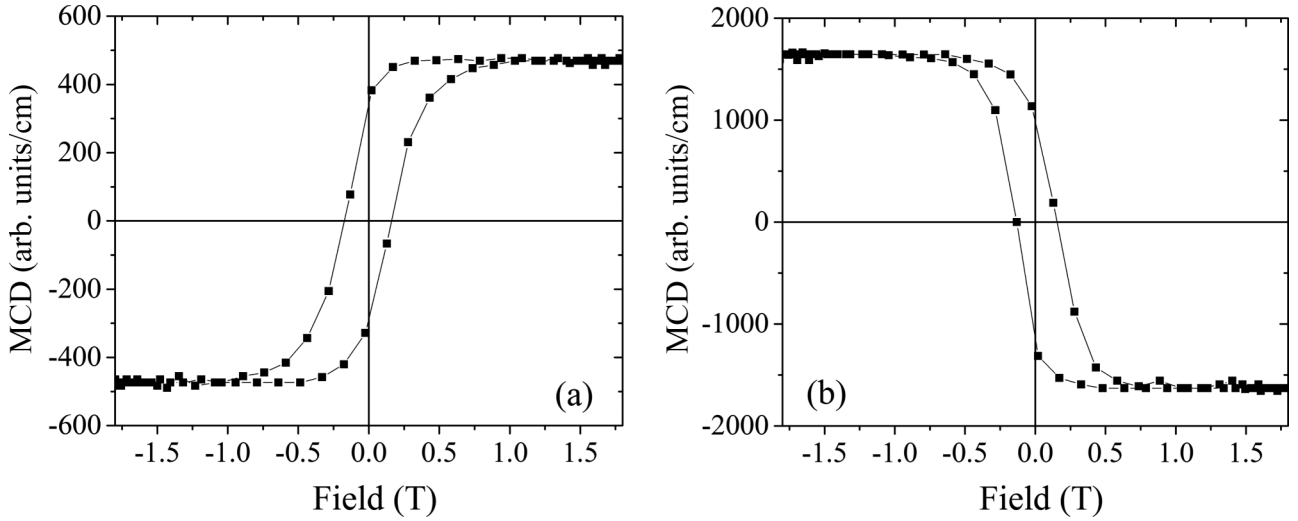

FIG. 10. The MCD loop taken at (a) 2.2 eV and (b) 3.2 eV (note that the reversal occurs because the MCD is negative). The linear background from the substrate has been subtracted.

loops obtained at different energies because it allows us to separate the contribution of the Fe_3O_4 nanoparticles from that from the polarized matrix. Loops taken at 2.2 eV and 3.2 eV are shown in Fig. 10 . In all cases a linear signal from the substrate has been subtracted; note that the loop taken at 3.2 eV is reversed because the MCD is negative at that energy. We note a comparison with Fig. 7 that shows that the loops taken at 2.2 eV and 3.2 eV approach $\pm$470 arb. units and $\mp$1600 arb. units, respectively, which are the values of the MCD at those energies. The values of the coercive field obtained from the MCD loops differ widely from those obtained in magnetometry (shown in Fig. 4). The coercive field at 2.2 eV is 1650 $\pm$ 50 Oe and 1400 $\pm$ 60 Oe at 3.2 eV. The peak in the ZFC magnetization plot is broad, indicating a wide distribution in the sizes of the nanoparticles. It appears that the very high value of the coercive field found at 2.2 eV in the MCD is coming almost entirely from large Fe_3O_4 nanoparticles and also that the magnetization from the polarized defect states in In_2O_3 contribute a relative large amount to the bulk magnetization.

VIII. DISCUSSION

The results presented here show that the results of the structural, transport, magnetic, and magneto-optical studies may be combined in a coherent manner to give a good understanding of these films. One of the characteristics of doped oxide films is that they often have low coercive fields, e.g., $\sim$100 Oe around RT. Some of the data on the films presented here show considerably higher coercive fields. The results for the 5% sample are summarized in Table III. It is clear that the values of the coercive field taken using MCD and the AHE are much higher than those taken using conventional magnetometry; this contrasts with measurements done on a sample with no nanoinclusions where the values were identical [42]. This difference arises because the nanoparticles give a disproportionally large contribution to the AHE and MCD. The largest value of the coercive field is obtained from the MCD at 2.2 eV that originates almost entirely from the nanoparticles. This can be used to estimate the amount of the signal from each type of measurement that originates directly from the nanoparticles; it is clearly substantial for the AHE but considerably less in the bulk magnetization as measured by the SQUID.

In particular, MCD has been shown to be a very powerful tool to separate the magnetic effects arising from nanoparticles from those coming from polarized electron bands in the In_2O_3 because the application of the Maxwell-Garnett theory showed there was a clear signal that was characteristic of pure Fe_3O_4 and an additional signal from close to the In_2O_3 band edge. The films doped with Fe alone showed an unusually high coercive field in plane at RT for an oxide sample (above 400 Oe). The data show that this is because they contain blocked nanoparticles of Fe_3O_4 and that the coercive field rises even higher below the Verwey transition, as shown in Figs. 2(c) and 2(d). The addition of 5% of Sn was found to reduce the concentration of nanoparticles to essentially zero, which is seen clearly in the MCD signal and by the fact that

TABLE III. A comparison of the coercive fields, given in Oersteds, for different measurements on the same sample: 5% Fe in In_2O_3 and also a comparison with the sample containing 5% Fe and 5% Sn.

	SQUID parallel	SQUID perpendicular	MCD loop 2.2 eV perp.	MCD loop 3.2 eV perp.	Anomalous Hall effect perp.	SQUID Including 5% Sn parallel
Room temperature	460 $\pm$ 50	530 $\pm$ 50	1650 $\pm$ 300	1460 $\pm$ 250	–	120 $\pm$ 10
Low temperature	650 $\pm$ 60	770 $\pm$ 70	–	–	1200 $\pm$ 200	205 $\pm$ 20

the anisotropy drops to a value normally associated with doped oxide films of 120 Oe at RT.

The films of Fe-doped In_2O_3 containing nanoparticles of Fe_3O_4 have contributions to the magnetism from the nanoparticles and also polarized electrons that are in the defect band formed from the oxygen vacancies. Important experimental findings are summarized below.

(1) The peak in the MCD at 2eV is entirely due to the nanoparticles. There is only a small reduction of the magnitude of this peak at remanence as seen in Fig. 8; however, the remanent magnetization shown in Table II is reduced by a much larger factor. This demonstrates that the bulk saturation magnetization has another contribution that is not due to the nanoparticles.

(2) The magnetization of the electrons in the indium oxide matrix contributes to the MCD due to the polarized defect band at ~3.2eV. This peak is considerably larger than the Maxwell-Garnett theory predicts for the contribution from the Fe_3O_4 so the balance comes from the polarized defect bands in the oxide. This is confirmed by the spectrum taken at remanence, which shows that the two components to the magnetization contribute differently to the signal at saturation and at remanence. The direction dependent saturation magnetization seen by SQUID measurements is also an indication of magnetism in the oxide or the interface layer.

(3) The SQUID magnetization measurements taken in plane and perpendicular to the plane show that there is no evidence for elongated nanoparticles in this material, unlike that seen earlier for Co nanoparticles [43]; this is supported by the fitting to the MCD spectra where a good fit was found for $L_{xx} = 0.33$.

(4) After the films have been annealed in vacuum, both the bulk magnetization and the magnitude of the MCD spectrum increase. The increase in the MCD peak due to nanoparticles is ~30%, which is not too different from the increase in the magnetization. However, the MCD signal showing polarized defect states increases much more, as can be seen from Fig. 9(b).

(5) The signal at 2 eV has been quenched in the sample with 5% of Sn, indicating that the fraction of nanoparticles has been dramatically decreased. This is accompanied by a sharp drop in the coercive field. The signal at ~3 eV is enhanced in these samples, corresponding to a larger carrier density.

IX. CONCLUSIONS

This study has shown that films of In_2O_3 with nanoparticles of Fe_3O_4 have very interesting properties. The saturation magnetization, coercive field, mobility, and conductivity are all high at RT. Since the nanoparticles did not coexist with added Sn, our study allowed us to compare films with and without the nanoparticles very directly.

A consistent understanding of the films was obtained from combining structural, magnetic, and optic data. The Fe_3O_4 nanoparticles were detected directly using EXAFS and were shown to give a very distinctive MCD spectrum. The volume fraction of the films that was occupied by the nanoparticles was determined by two techniques, and the results were shown to be in approximate agreement. This is very significant because they measure different quantities: EXAFS is a structural measurement that cannot make any predictions about magnetism, and the MCD measured the volume fraction that had a dielectric function that was characteristic of bulk Fe_3O_4. The similarity of these measurements means that most of the Fe ions with the coordination of Fe_3O_4 were also magnetic with approximately the bulk dielectric functions. It was found that in this case the fraction of Fe_3O_4 varied smoothly as the concentration of Fe was increased.

An additional feature of the study was the use of SQUID magnetometry and MCD data to indicate that there were two separate contributions to the magnetization from the nanoparticles and from the oxide host that had different dependence on the external field. The oxide component is responsible for the smaller coercive field seen by SQUID magnetometry and also for the difference between the observed saturation magnetization and that expected from the nanoparticles [as shown in Fig. 5(b)]. It was found that the magnetization of the nanoparticles was increased by vacuum annealing but suppressed by the addition of Sn. On the other hand, the oxide contribution depended on the carrier density and so was enhanced by both the addition of Sn and vacuum annealing.

The presence of the Fe_3O_4 nanoparticles enhances the magnetization and the coercive field is still substantial at RT. In addition, there is a contribution from the electrons in a donor band, which may be associated with grain boundaries or interfaces. Annealing the films in vacuum increased the density of states of the donor band; hence, the strength of the MCD signal at the band edge, also the fraction of Fe_3O_4 nanoparticles, increased slightly. The effects of adding Sn were to increase the carrier concentration and hence the MCD signal at the band edge as expected; however, the unexpected result was the dramatic fall in the density of nanoparticles after Sn was added. The thin films investigated show great promise for technological exploitation as they combine a large coercive field at RT with high carrier density, low resistance, and polarized carriers.

ACKNOWLEDGMENTS

This research was funded by the UK Engineering and Physical Sciences Research Council (United Kingdom) Grant No. EP/D070406/1 and a studentship for AMHRH and also King Abdulaziz City for Science and Technology, KACST (Saudi Arabia). The Advanced Photon Source is supported by the US Department of Energy—Basic Energy Sciences (USA) under Contract No. DE-AC02–06CH1135. Pacific Northwest Consortium and X-ray Science Division facilities are also supported by the Canadian Light Source and its funding partners, the University of Washington, and the Advanced Photon Source.

[1] N. Izyumskaya, Y. Alivov, and H. Morkoc, Crit. Rev. Solid State Sci. **34**, 89 (2009).

[2] S. A. Wolf, D. D. Awschalom, R. A. Buhrman, J. M. Daughton, S. von Molnár, M. L. Roukes, A. Y. Chtchelkanova, and D. M. Treger, Science **294**, 1488 (2001).

[3] C. Nunes de Carvalho, G. Lavareda, A. Amaral, O. Conde, and A. R. Ramos, J. Non-Cryst. Solids **352**, 2315 (2006).

[4] J.-H. Lee, S.-Y. Lee, and B.-O. Park, Mater. Sci. Eng. B **127**, 267 (2006).

[5] H. Han, J. W. Mayer, and T. L. Alford, J. Appl. Phys. **99**, 123711 (2006).

[6] H. Han, D. Adams, J. W. Mayer, and T. L. Alford, J. Appl. Phys. **98**, 083705 (2005).

[7] P. D. C. King, T. D. Veal, F. Fuchs, C. Y. Wang, D. J. Payne, A. Bourlange, H. Zhang, G. R. Bell, V. Cimalla, O. Ambacher, R. G. Egdell, F. Bechstedt, and C. F. McConville, Phys. Rev. B **79**, 205211 (2009).

[8] P. D. C. King, T. D. Veal, D. J. Payne, A. Bourlange, R. G. Egdell, and C. F. McConville, Phys. Rev. Lett. **101**, 116808 (2008).

[9] F.-X. Jiang, X.-H. Xu, J. Zhang, H.-S. Wu, and G. A. Gehring, Appl. Surf. Sci. **255**, 3655 (2009).

[10] F.-X. Jiang, X.-H. Xu, J. Zhang, X.-C. Fan, H.-S. Wu, M. Alshammari, Q. Feng, H. J. Blythe, D. S. Score, K. Addison, M. Al-Qahtani, and G. A. Gehring, J. Appl. Phys. **109**, 053907 (2011).

[11] X.-H. Xu, F.-X. Jiang, J. Zhang, X.-C. Fan, H.-S. Wu, and G. A. Gehring, Appl. Phys. Lett. **94**, 212510 (2009).

[12] S. C. Li, P. Ren, B. C. Zhao, B. Xia, and L. Wang, Appl. Phys. Lett. **95**, 102101 (2009).

[13] A. Singhal, S. N. Achary, J. Manjanna, O. D. Jayakumar, R. M. Kadam, and A. K. Tyagi, J. Phys. Chem. C **113**, 3600 (2009).

[14] Y. K. Yoo, Q. Xue, H.-C. Lee, S. Cheng, X.-D. Xiang, G. F. Dionne, S. Xu, J. He, Y. S. Chu, S. D. Preite, S. E. Lofland, and I. Takeuchi, Appl. Phys. Lett. **86**, 042506 (2005).

[15] J. He, S. Xu, Y. K. Yoo, Q. Xue, H.-C. Lee, S. Cheng, X.-D. Xiang, G. F. Dionne, and I. Takeuchi, Appl. Phys. Lett. **86**, 052503 (2005).

[16] J. Philip, A. Punnoose, B. I. Kim, K. M. Reddy, S. Layne, J. O. Holmes, B. Satpati, P. R. LeClair, T. S. Santos, and J. S. Moodera, Nat Mater **5**, 298 (2006).

[17] O. Takahiro, K. Toshio, T. Hidekazu, K. Tomoji, O. Masaoki, O. Koichi, and K. Shigemi, Japanese J. Appl. Phys. **45**, L957 (2006).

[18] K. Okada, S. Kohiki, M. Mitome, H. Tanaka, M. Arai, M. Mito, and H. Deguchi, ACS Applied Materials & Interfaces **1**, 1893 (2009).

[19] Q. Li, L. Wei, Y. Xie, T. Zhou, G. Hu, S. Yan, J. Jiao, Y. Chen, G. Liu, and L. Mei, Nanoscale **5**, 2713 (2013).

[20] W. Wang, M. Yu, M. Batzill, J. He, U. Diebold, and J. Tang, Phys. Rev. B **73**, 134412 (2006).

[21] K. Liu, L. Zhao, P. Klavins, F. E. Osterloh, and H. Hiramatsu, J. Appl. Phys. **93**, 7951 (2003).

[22] H. Zeng, C. T. Black, R. L. Sandstrom, P. M. Rice, C. B. Murray, and S. Sun, Phys. Rev. B **73**, 020402 (2006).

[23] S. Jang, W. Kong, and H. Zeng, Phys. Rev. B **76**, 212403 (2007).

[24] S. Qi, F. Jiang, J. Fan, H. Wu, S. B. Zhang, G. A. Gehring, Z. Zhang, and X. Xu, Phys. Rev. B **84**, 205204 (2011).

[25] S.-j. Hu, S.-s. Yan, X.-l. Lin, X.-x. Yao, Y.-x. Chen, G.-l. Liu, and L.-m. Mei, Appl. Phys. Lett. **91**, 262514 (2007).

[26] D. Bérardan, E. Guilmeau, and D. Pelloquin, J. Magn. Magn. Mater. **320**, 983 (2008).

[27] Z. Quan, W. Liu, X. Li, X. Xu, K. Addison, D. S. Score, and G. A. Gehring, Materials Letters **65**, 2982 (2011).

[28] D. S. Score, M. Alshammari, Q. Feng, H. J. Blythe, A. M. Fox, G. A. Gehring, Z.-Y. Quan, X.-L. Li, and X.-H. Xu, J. Phys.: Conf. Ser. **200**, 062024 (2010).

[29] P. Brahma, S. Banerjee, D. Das, P. K. Mukhopadhyay, S. Chatterjee, A. K. Nigam, and D. Chakravorty, J. Magn. Magn. Mater. **246**, 162 (2002).

[30] D. Stroud, Phys. Rev. B **12**, 3368 (1975).

[31] M. Venkatesan, C. B. Fitzgerald, J. G. Lunney, and J. M. D. Coey, Phys. Rev. Lett. **93**, 177206 (2004).

[32] B. C. Zhao, B. Xia, H. W. Ho, Z. C. Fan, and L. Wang, Physica B: Condensed Matter **404**, 2117 (2009).

[33] H. S. Hsu, C. P. Lin, S. J. Sun, and H. Chou, Appl. Phys. Lett. **96**, 242507 (2010).

[34] R. Swanepoel, J. Phys. E **16**, 1214 (1983).

[35] V. Senthilkumar, P. Vickraman, M. Jayachandran, and C. Sanjeeviraja, Vacuum **84**, 864 (2010).

[36] A. J. Behan, J. R. Neal, R. M. Ibrahim, A. Mokhtari, M. Ziese, H. J. Blythe, A. M. Fox, and G. A. Gehring, J. Magn. Magn. Mater. **310**, 2158 (2007).

[37] C. Clavero, B. Sepulveda, G. Armelles, Z. Konstantinovic, M. G. del Muro, A. Labarta, and X. Batlle, J. Appl. Phys. **100**, 074320 (2006).

[38] J. S. Ahn, K. H. Kim, T. W. Noh, D.-H. Riu, K.-H. Boo, and H.-E. Kim, Phys. Rev. B **52**, 15244 (1995).

[39] W. F. J. Fontijn, P. J. van der Zaag, M. A. C. Devillers, V. A. M. Brabers, and R. Metselaar, Phys. Rev. B **56**, 5432 (1997).

[40] F.-X. Jiang, Q. Feng, Z.-Y. Quan, R.-R. Ma, S. M. Heald, G. A. Gehring, and X.-H. Xu, Mater. Res. Bull. **48**, 3178 (2013).

[41] A. M. H. R. Hakimi, M. G. Blamire, S. M. Heald, M. S. Alshammari, M. S. Alqahtani, D. S. Score, H. J. Blythe, A. M. Fox, and G. A. Gehring, Phys. Rev. B **84**, 085201 (2011).

[42] H. Kim, M. Osofsky, M. M. Miller, S. B. Qadri, R. C. Y. Auyeung, and A. Pique, Appl. Phys. Lett. **100**, 032404 (2012).

[43] N. Jedrecy, H. J. von Bardeleben, and D. Demaille, Phys. Rev. B **80**, 205204 (2009).